scientific reports

OPEN

Facile synthesis of flower shaped magnesium ferrite (MgFe$_2$O$_4$) impregnated mesoporous ordered silica foam and application for arsenic removal from water

Md. Jamal Uddin[1]✉ & Yeon-Koo Jeong[2]✉

Magnesium ferrite (MF$_{0.33}$) impregnated flower-shaped mesoporous ordered silica foam (MOSF) was successfully synthesized in present study. MOSF was added with precursor solution of MF$_{0.33}$ during MF$_{0.33}$ synthesis which soaked the materials and further chemical changes occurred inside the pore. Therefore, no additional synthesis process was required for magnesium ferrite impregnated mesoporous ordered silica foam (MF$_{0.33}$-MOSF) synthesis. MF$_{0.33}$-MOSF showed higher morphological properties compared to other magnesium ferrite modified nanomaterials and adsorbed arsenic III [As(III)] and arsenic V [As(V)] 42.80 and 39.73 mg/g respectively. These were higher than those of other Fe-modified adsorbents at pH 7. As MOSF has no adsorption capacity, MF$_{0.33}$ played key role to adsorb arsenic by MF$_{0.33}$-MOSF. Data showed that MF$_{0.33}$-MOSF contain about 2.5 times lower Fe and Mg than pure MF$_{0.33}$ which was affected the arsenic adsorption capacity by MF$_{0.33}$-MOSF. Adsorption results best fitted with Freundlich isotherm model. The possible mechanism of arsenic adsorption might be chemisorption by electrostatic attraction and inner or outer-sphere surface complex formation.

Arsenic toxicity is a well-known global problem affecting millions of people each year. Naturally arsenic comes from ground water. The use of ground water as drinking and irrigation purpose causes arsenic transfer to human health. Arsenic can cause several health dieses like keratosis, hyperkeratosis, melanosis, leucomelanosis, dorsum, and even cancer[1]. Governments are investing a lot of budgets for removal of arsenic from water. Among different technologies, adsorption is an efficient technology for arsenic removal from water[2]. Research data proved that iron-based adsorbents performed well over other adsorbents in arsenic removal[3]. However, modification through impregnation, coating and functionalization of iron adsorbents with porous material improved adsorbent characteristics which enhanced As removal efficiency[4–7].

Different kinds of porous materials have been used for water treatment solely or as a composite with other material so far. Sand, clay, zeolite, activated carbon and silica are typical porous materials used for arsenic removal from water through adsorption process[8,9]. There were different advantages for using porous material as support or carrier material. Firstly, porous materials can reduce the aggregation of nanomaterials during adsorption process. This phenomenon decreases surface area and active sites of the adsorbent. Secondly, selectivity and catalytic activity of adsorbents for pollutant adsorption can be affected by the textural properties of the carrier material. Pollutants can form a thin layer on the pore channels or walls and be attached swiftly. Thirdly, encapsulation and impregnation of active nanomaterials into the pore and cavities of porous material increases the stability and dispersion of nanomaterials in catalysis process. Finally, for more flexibility, pore dimensions, morphology and structure of the porous materials can be designed as per requirement of the research. Activated carbon, zeolite, activated alumina can show upper three advantages but the final advantage is the specialty for mesoporous silica material which made this material more efficient over others[10].

Porous silica material were considered as ideal material in different application because of exceptionally large surface area, thermal and chemical stability, high pore volume, low density, high selectivity and flexibility which can be modified using different organic and inorganic functional groups[10,11]. Among different type

[1]Department of Soil and Environmental Sciences, University of Barishal, Barishal 8254, Bangladesh. [2]Department of Environmental Engineering, Kumoh National Institute of Technology, 61 Daehak-ro, Gumi, Gyeongbuk 39177, Republic of Korea. ✉email: jamal_swedu@yahoo.com; jeongyk@kumoh.ac.kr

of porous silica materials, macro and mesoporous silica foam (MOSF) was found most suitable for pollutant removal from water through adsorption. Yang et al.[12] synthesized lanthanum coated MOSF which removed 96% phosphorus within 30 min. They further modified MOSF with γ-Fe_2O_3 nanoparticles and applied for As(III) and As(V) removal from water. Data revealed that maximum 34.8% γ-Fe_2O_3 nanoparticles dispersed on pore walls of MOSF which adsorbed 248 and 320 mg/g As(III) and As(V) [Initial conc. of As(III) and As(V) was 560 and 600 mg/l] respectively[13].

Iron was found most efficient element for arsenic removal through adsorption process[1]. Among Fe-based adsorbents, spinel ferrites exhibited exceptional performance in pollutant removal during water treatment. However, researchers found health toxicity because of cobalt ferrites. But there were no data found on magnesium ferrite ($MgFe_2O_4$) related toxicity in literature. In addition, magnesium plays essential functional activity inside human body. Besides that, among all spinel ferrites, magnesium ferrite showed better performance in pollutant removal through adsorption because of easy availability, safe handling, large surface area, tunable porosity and economically viable properties[2,14]. However, nanomaterials have some negative properties during adsorption such as aggregation and separation. Jung et al.[15] showed that $MgFe_2O_4$ /Biochar composite adsorbed higher amount of phosphate than $MgFe_2O_4$ nanoparticles. Karthikeyan et al.[16] also reported that modified $MgFe_2O_4$ was performed more efficiently for toxic ions removal than single $MgFe_2O_4$ nanoparticles. Based on the literature data, it was found that the modified material showed more stable morphological properties. In addition, modification increased the adsorptive site and influenced on pH_{PZC} that removed more toxic ions from solution. Furthermore, modification of magnesium ferrite not only increased adsorption capacity but also increased the stability and pollutant selectivity during adsorption process[15-17]. Considering the exceptional properties of MOSF in literature, present research was structured to develop a new composite material that might remove pollutants from water efficiently[10].

Tile date, there was no literature found based on $MgFe_2O_4$ modified MOSF composite material. Very few research data were found on adsorptive arsenic removal from water using magnesium ferrite nanomaterials[14,18,19]. In addition, MOSF might increase $MgFe_2O_4$ nanomaterials stability and adsorption capacity which was the main objective of this research[12,13]. Therefore, considering efficiency and economic value, a simple Solvothermal method was followed for magnesium ferrite impregnated MOSF synthesis in present study and applied for arsenic removal from water.

Materials and methods

All the chemicals and reagents used in present study were ACS-grade and supplied by Daihan Scientific, Republic of Korea. $MgFe_2O_4$ nanomaterial was synthesized by following a method with major modifications in different experimental factors[19,20]. To follow the ratio of Fe:Mg = 0.67:0.33, appropriate amount of anhydrous ferric chloride ($FeCl_3$) and magnesium chloride ($MgCl_2$) were dissolved in 70 ml ethanol (C_2H_6O). After that, 10 ml of just prepared 2.03 M sodium hydroxide-ethanol (NaOH-C_2H_6O) mixture added to the solution. To make a homogenized solution, the mixed solution was taken under a Sonicator for 1 h at 25 ± 5 °C temperature. Sonicator probe height, amplitude and temperature were carefully maintained for all runs. The homogenized solution mixture was taken into a Teflon-line autoclave made of stainless steel and closed it tightly. Then the autoclave was kept in a convective oven for 8 h at 200 °C temperature. The autoclave was naturally cooled to room temperature. After that, the mixture was transferred into a 100 ml beaker and washed using deionized water with the help of magnetic stirrer. The washing process was continued until the mixture was free from sodium chloride. The final precipitate was transferred to a ceramic cup and taken into the oven for 12 h at 80 °C temperature. After that time period, the ceramic cup was kept in a desiccator carefully and naturally cooled. Next, the dried materials were grounded using a ceramic mortar where a dark brown finer material produced. Finally, the material was transferred into a dark glass bottle and preserved for characterization and adsorption experiments.

The method for mesoporous silica foam synthesis under present study was followed the method described by Wang et al.[21] with some minor changes. At first, 1 g of P123 was measured in a beaker and kept it in a water bath having 35 °C. Then, 30 ml of 0.40 M sodium sulphate (Na_2SO_4) solution was added and stirred continuously. Subsequently, 31 ml of 0.02 M sodium acetate-acetic acid buffer solution was added under continuous stirring. The mixture was stirred until a homogenous mixture solution formed. Next, 1.48 ml of tetramethyl orthosilicate (TMOS) solution was added to the solution mixture and stirred for 5 min further. The beaker containing solution mixture was kept in an incubator under 35 °C. After 24 h of incubation, the mixture was sealed in a teflon-lined-autoclave and leaved it in the oven for another 24 h at 100 °C. After that, the autoclave was naturally cooled and the mixture was washed with water until it became sodium free. Finally, the white precipitate was air dried and calcined at 550 ˚C temperature for 5 h in a muffle furnace. The white colored material then was cooled in a desiccator and preserved for further analysis.

The impregnation in this study was very simple and no further chemicals were required. Appropriate amount of anhydrous $FeCl_3$ and $MgCl_2$ were mixed with synthesized MOSF in 70 ml ethanol under sonication. After 30 min of sonication, freshly prepared NaOH solution (10 ml) was added to the mixture drop wise under continuous sonication. After 1 h of sonication, the mixture was sealed in the teflon-lined-autoclave and heated at 200 °C temperature for 8 h in the oven. Next, the naturally cooled mixture was washed with deionized water for several times until the mixture was become sodium chloride (NaCl) free with the help of 2 min continuous sonication and 10 min magnetic stirring. The drying and grinding process of the washed material was same as magnesium ferrite synthesis. The magnesium ferrite nanomaterial having molar ratio of magnesium and iron 0.33:0.67 was expressed as $MF_{0.33}$ and this was incorporated into MOSF. The end material was used for characterization and adsorption process.

Characterization

Powder X-ray diffraction (XRD) pattern (Rigaku Japan, using filtered Cu Kα radiation) of the synthesized material was determined for crystal phase identification. The average crystallographic size of synthesized material was calculated from the most intense peaks on XRD spectra using Scherrer's equation. The elemental composition and morphology was investigated using field emission electron microscopy (SEM; MAIA3 TESCAN) functioning with an energy dispersive X-ray (EDS). Chemical composition and bonding nature were proved by Fourier transform-infrared spectroscopy (FT-IR; BRUKER). Magnetic properties of the synthesized materials were analyzed by vibrating sample magnetometer (VSM, Lake Shore Cryotronics, Inc.). N_2 adsorption–desorption isotherm was recorded from micromeritics. Average pore size, shape, volume and specific surface area were obtained using Barrett-Joyner-Halenda (BJH) and Brunauer–Emmett–Teller (BET) method.

Adsorption experiments

To observe the adsorption efficiency of $MF_{0.33}$-MOSF, nine sets (1, 5, 10, 25, 50, 100, 150, 200 and 300 mg/l) of As(III) and eight sets (1, 5, 10, 20, 40, 60, 100 and 130 mg/l) of As(V) concentration were prepared from stock solution (1000 mg/l). 1.0 g/l adsorbent dose was applied. pH values were measured before and after adding adsorbent. Dilute hydrochloric acid (HCl) and NaOH were used to adjust pH 7 after adsorbents addition. The conical flasks containing arsenic solution and adsorbent were kept in a shaking incubator for 12 h. The incubator was operated at 300 ± 5 rpm and temperature was controlled at 25 °C. Next, the mixture solutions were centrifuged for 1 h at 4000 rpm to separate solids. Then, approximately 20 ml clear solution was transferred to plastic tube. To avoid further oxidation, 1 drop of concentrated HCl was added to each solution tube and stored. These solutions were used to determine equilibrium As(III) and As(V) concentration using inductively coupled plasma optical emission spectroscopy (ICP-OES). Adsorption capacity of synthesized $MF_{0.33}$-MOSF nanomaterial was computed according to the equation given below[22]:

$$\text{Arsenic adsorption capacity, } q_e = \frac{V}{m} \times (C_0 - C_e) \tag{1}$$

where, C_0 (mg/l) is the initial concentration of As(III) and As(V), C_e (mg/l) is the equilibrium concentration of As(III) and As (V), V (l) for volume, m (g) for adsorbent dose and q_e (mg/g) for adsorption capacity at equilibrium respectively.

To quantify maximum arsenic adsorption capacity and possible arsenic adsorption mechanism by synthesized $MF_{0.33}$ impregnated MOSF, two adsorption isotherm models have been applied named Freundlich (Freundlich, 1906) adsorption isotherm model and Langmuir (Langmuir, 1916) adsorption isotherm model.

The Freundlich adsorption isotherm model can be expressed as follows:

$$q_e = K_f C_e^{\frac{1}{n}} \tag{2}$$

where, q_e is the arsenic adsorption capacity by adsorbent at equilibrium (mg/g), C_e is the equilibrium arsenic concentration in water (mg/l), K_f ($mg^{1-1/n}l^{1/n}g^{-1}$) and n is the Freundlich empirical constants which are related to the maximum arsenic adsorption and the 1/n is the heterogeneity factor of the nanoadsorbent representing the strength of adsorption. The value of n should be lie between 1 and 10 for favorable adsorption process[23].

The Langmuir adsorption isotherm model can be expressed as follows:

$$q_e = \frac{q_m K_L C_e}{(1 + K_L C_e)} \tag{3}$$

where, K_L (l/mg) designated as Langmuir adsorption constant, C_e is the equilibrium arsenic concentration (mg/l), q_e (mg/g) is the arsenic adsorption capacity at equilibrium and q_m (mg/g) represents maximum adsorption capacity of As(III) and As(V) on $MF_{0.33}$-MOSF. The affinity of arsenic toward binding site is related with K_L.

Determination of pH_{PZC}

Point of zero charge (pH_{PZC}) of $MF_{0.33}$-MOSF nanomaterial was identified through pH Drift method[24]. In short, based on pH, 10 different sets of vial (pH 3–12) were prepared by adding 15 ml NaCl solution having 0.1 M concentration. pH 3–12 was made by using HCl or NaOH solutions (for pH < 7, HCl and for pH ˃ 7, NaOH). Subsequently, 0.015 g of $MF_{0.33}$-MOSF nanomaterial was added to each vial. The vials were stirred 4 h using a magnetic stirrer and kept it in a temperature (25 °C) controlled incubator for 24 h. The final pH of each vials were measured and an initial pH vs pH change (ΔpH) graph was made. The line pH-ΔpH crossed the point of pH zero line is the pH_{PZC} of the material.

Ethical approval

This is an original research and has not been submitted elsewhere at the same time. The whole research compiled in a single manuscript which submitted to *Scientific Reports*. A new material named MOSF modified MF was first time prepared and applied for arsenic removal by the authors. Before submission, the manuscript was checked for plagiarism using Turnitin software.

Results and discussion
Characteristics of magnesium ferrite impregnated MOSF
XRD

The XRD spectra of synthesized $MF_{0.33}$, MOSF and $MF_{0.33}$-MOSF material at 2θ scale ranging from 10° to 80° were shown in Fig. 1. For MOSF, only one peak was found at 2θ = 22° on the XRD spectra which was representative for the formation of amorphous silica[25]. The peak pattern found in $MF_{0.33}$ demonstrated successful synthesis of single phase [S/M (PDF-2 release 2020 RDB)] cubic shape magnesium ferrite spinels which belongs to space group Fd3m (227:Fd-3 m:2; a = 8.39913 Å). Figure 1 showed diffraction peaks at 2θ = 18.31 (111), 30.09 (220), 35.40 (311), 43.05 (400), 53.35 (422), 56.95 (511), 62.53 (440), 71.00 (620) and 74.10 (533) which was properly fitted with inorganic crystal structure database (ICSD-01-076-9733). $MF_{0.33}$-MOSF produced 6 peaks on the XRD spectra. The peak at 2θ = 22° confirmed the amorphous silica and 2θ = 31.10 (220), 35.30 (311), 43.43 (400), 56.46 (511) and 62.64 (440) were attributed to the spinel magnesium ferrite nanomaterial, which was appropriately fitted with standard XRD planes for cubic-spinel shaped $MgFe_2O_4$ nanomaterial card number ICSD-01-076-9733.

Therefore, based on the comparison results, the new synthesized material contained both amorphous silica phase and magnesium ferrite spinels. These data also confirmed that magnesium ferrite crystals were well established in MOSF structure. Intense peaks of the XRD plane were used to calculate average crystallite size according to Debye–Scherrer's formula[26,27].
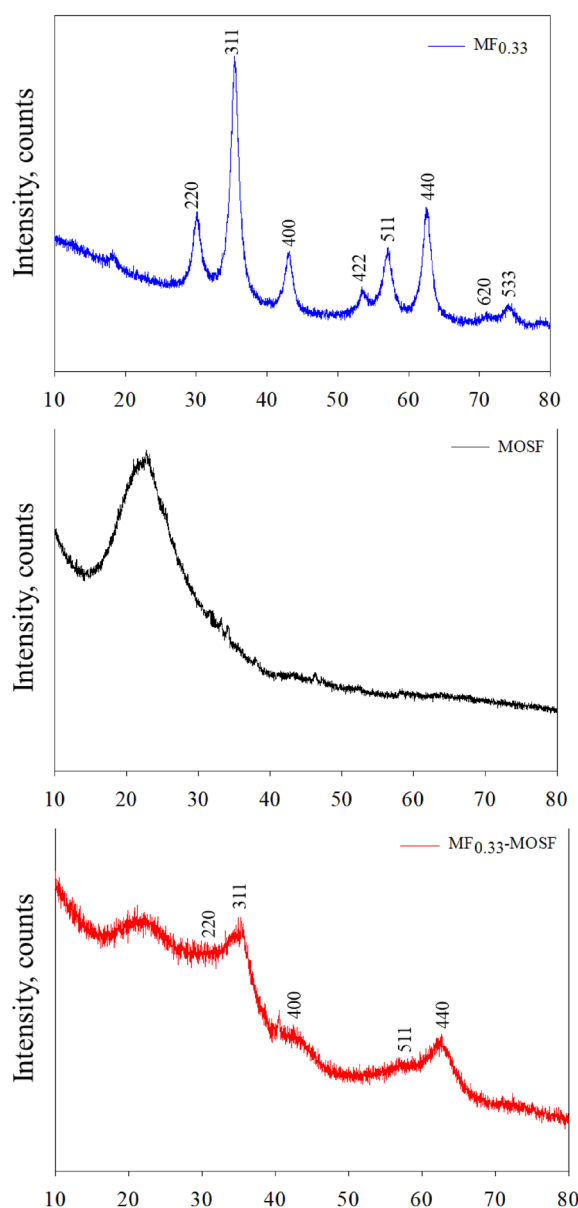
According to the Debye–Scherrer's formula,

Figure 1. XRD spectra of synthesized nanomaterials.

$$\text{Crystalline size,} \quad D \quad = \quad (K\lambda / \beta \cos\theta) \qquad (4)$$

where, D (nm) average crystalline size, K ($K = 0.89$) is considered as Scherer's constant, λ (Å) represents the applied wavelength of X-ray, β (radian) represents as the full width at half maximum (FWHM) of the diffraction peak and θ represents diffraction angle produced by the peak.

The calculated average crystallite size was found 5.85, 0.75 and 1.84 nm for $MF_{0.33}$, MOSF and $MF_{0.33}$-MOSF respectively. There were no other peaks found on the XRD plane which confirmed that the material synthesized under present research is in single phase state with high purity.

N_2 adsorption–desorption isotherms

Specific surface area, average pore volume and pore size of $MF_{0.33}$, MOSF and $MF_{0.33}$-MOSF were measured through N_2 adsorption–desorption isotherm analysis, as represented in Fig. 2. Comparing with international union of pure and applied chemistry (IUPAC) provided classification of hysteresis loop, the pattern displayed in N_2 adsorption–desorption curves were matched with single mode IV which belongs to H1 hysteresis loop. Based on IUPAC classification, this type of hysteresis mode corresponding to the presence of abundant mesoporous pores[28]. The Barrett-Joyner-Halenda (BJH) pore size distribution pattern revealed average pore diameter of $MF_{0.33}$, MOSF and $MF_{0.33}$-MOSF were 4.17, 11.41 and 6.05 nm respectively (Table S1). $MF_{0.33}$ impregnation in MOSF decreased the pore diameter, which might be resulted from the incorporation of $MF_{0.33}$ particles in pore of MOSF. The Brunauer–Emmett–Teller (BET) total pore volume and specific surface area of mesoporous $MF_{0.33}$, MOSF and $MF_{0.33}$-MOSF nanomaterials were 0.2083, 0.8012, 0.4684 cm^3/g and 200.36, 412.86, 427.04 m^2/g respectively. Owing to impregnation, BET surface area was increased, which indicated that the particles size of
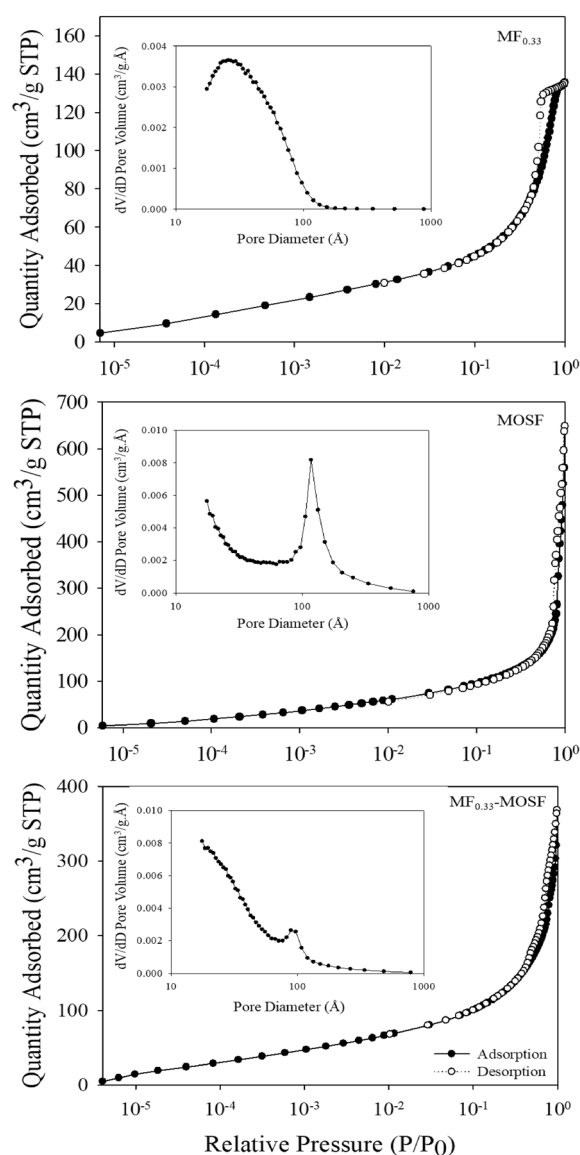

Figure 2. N_2 adsorption–desorption isotherms of $MF_{0.33}$, MOSF and $MF_{0.33}$-MOSF.

$MF_{0.33}$-MOSF was decreased after impregnation. The average nanoparticle size found by BET analysis (29.95, 14.53 and 14.05 for $MF_{0.33}$, MOSF and $MF_{0.33}$-MOSF respectively) also supported the increment of surface area. The decrease in total pore volume in impregnated material might be also resulted from the impregnated magnesium ferrite in MOSF. Therefore, the $MF_{0.33}$-MOSF nanomaterial showed exceptionally large surface area, high pore volume and mesoporous pore size that would be an efficient adsorbent for pollutant removal from water.

FTIR

To recognize the bonding types, nature and functional groups of the $MF_{0.33}$, MOSF and $MF_{0.33}$-MOSF nanomaterials, FTIR analysis was performed and results showed in Fig. 3. The IR data was collected in range of 400–4500/cm of wavenumber. The distinctive adsorption peaks of $MF_{0.33}$ nanomaterial were appeared at 3416, 1637, 1384, 1034, 590 and 433/cm region were identical to the literature data for magnesium ferrite nanomaterial[14,29]. The broader peak appeared at 3416/cm and the sharp peak turned up at 1637/cm region were associated with stretching and bending vibrations of –O–H groups and surface adsorbed water (H_2O) by hydrogen bond on $MF_{0.33}$ surface. The other sharp peaks produced at 1384/cm and 1034/cm region of the spectra were assigned to deformation and bending vibrations of metal hydroxide ($M\text{-}OH^-$), which coordinated to Fe^{3+} or Mg^{2+}. The intense peaks appeared at 590/cm and 433/cm were related to the innate vibrations of octahedral and tetrahedral metal oxides ($M\text{–}O$)[29]. For MOSF, the peak at 3434/cm was attributed to stretching vibration of –OH on the MOSF surface. The bending vibration of the adsorbed water on the surface absorbed the light 1629/cm. Additionally, the peak at 1091/cm and 810/cm were attributed to asymmetric and symmetric stretching vibrations of Si–O–Si bond. Furthermore, the peak produced at 465/cm was assigned to the structural SiO_4 tetrahedra[30,31]. The FTIR
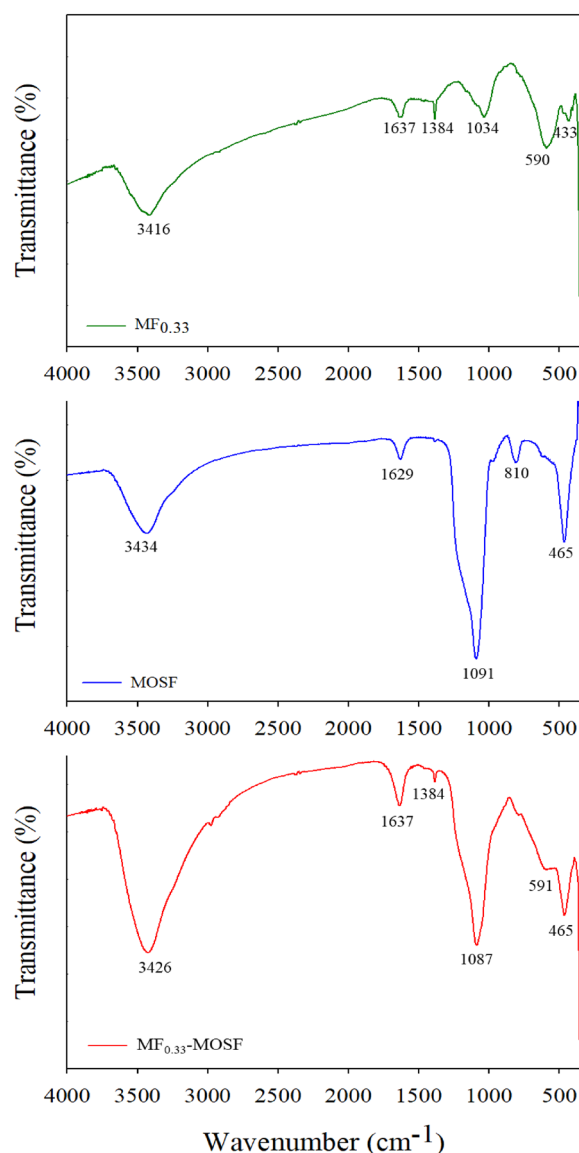

Figure 3. FTIR spectra of $MF_{0.33}$, MOSF and $MF_{0.33}$-MOSF nanomaterials.

spectra for $MF_{0.33}$-MOSF nanomaterial showed almost all the chemical bonds observed in $MF_{0.33}$ and MOSF. These results also confirmed the successful impregnation of $MF_{0.33}$ in MOSF.

SEM–EDS
Surface morphology of $MF_{0.33}$, MOSF and $MF_{0.33}$-MOSF nanomaterials were observed through SEM analysis (Fig. 4). The synthesis method of $MF_{0.33}$ and $MF_{0.33}$-MOSF nanomaterial was divided into four steps which were homogenization, thermal treatment, washing and drying. The synthesized materials after thermal treatment remain as finer particles which suspended rapidly in water during washing of the material for NaCl removal. However, the nanomaterials formed small agglomerates after 12 h heating in the oven for drying. Therefore, naturally cooled agglomerates were taken into a ceramic mortar and grounded to finer particles. The SEM image
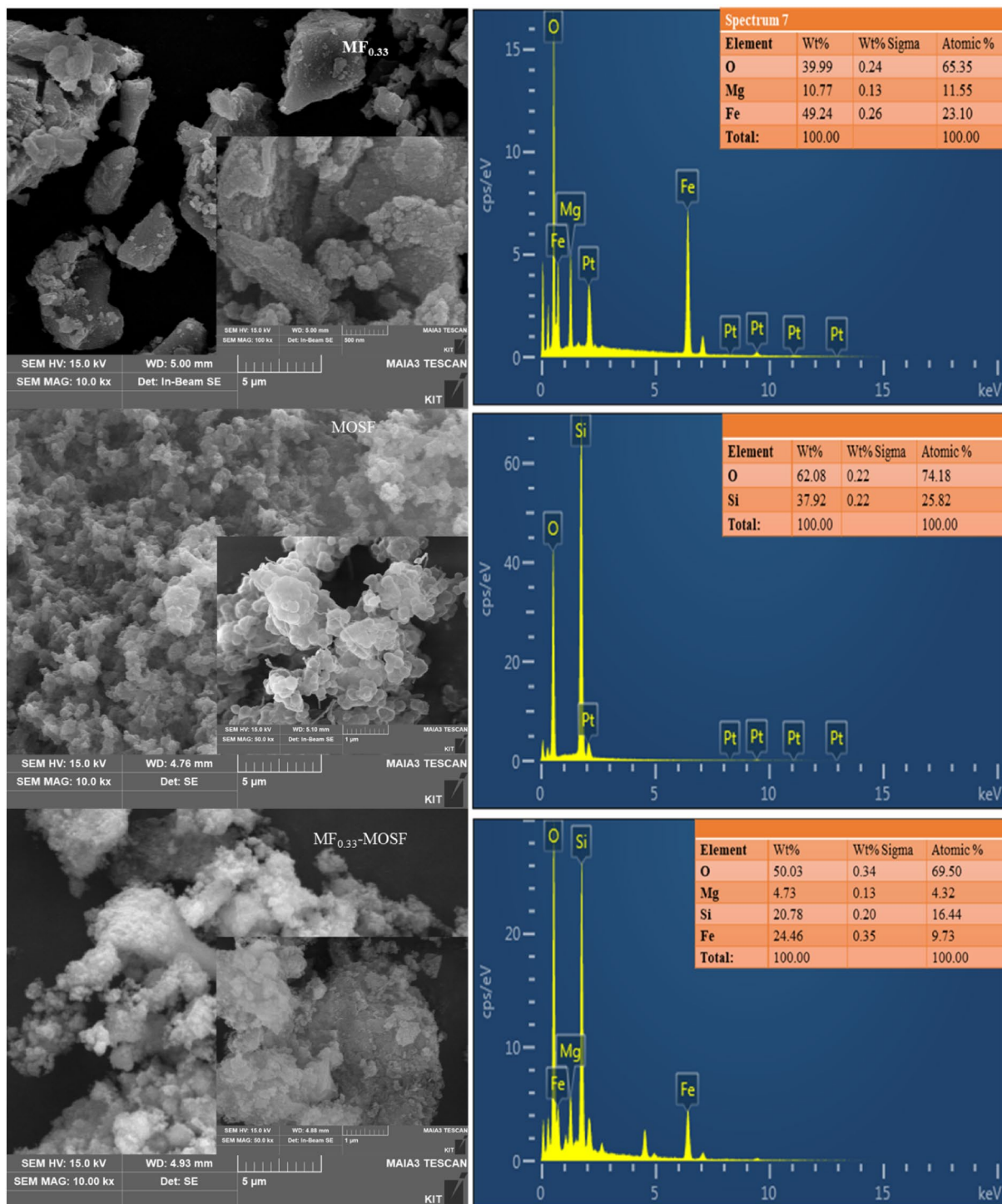

Figure 4. SEM–EDS of $MF_{0.33}$, MOSF and $MF_{0.33}$-MOSF nanomaterial.

of MOSF nanomaterials was showed flower shape in appearance and there was no need to grind. Because of grounding, the agglomerates of $MF_{0.33}$ were broken through the boundary line between the cubic spinel shape particles which were shown in Fig. 4. Although, the impregnated material showed similar agglomerates like $MF_{0.33}$ but clear spinels could not be found in the impregnated materials like $MF_{0.33}$ which might be due the growth of $MF_{0.33}$ spinels inside the pores of flower shape MOSF nanomaterial. This also supported the data found in N_2 adsorption–desorption isotherm analysis. Based on that data, the MOSF nanomaterial was found mesoporous having large pores. And it was also found that the size of MOSF particles were smaller than that of $MF_{0.33}$. After impregnation, the pore size and pore volume of MOSF nanomaterial decreased and a new shape was found in $MF_{0.33}$-MOSF image which has similarities with flower shape MOSF.

For the evaluation of elemental composition in each nanomaterial, EDS analysis has been done (Fig. 4). The EDS analysis of $MF_{0.33}$-MOSF proved the presence of Si, Fe, Mg and O element, which came from $MF_{0.33}$ and MOSF. The $MF_{0.33}$ nanomaterial contains 23.10% of Fe and 11.55% (atomic weight base) of Mg. But after impregnation of $MF_{0.33}$ in MOSF by 1:1 ratio, $MF_{0.33}$-MOSF contain approximately 2.37 times lower Fe and 2.67 times lower Mg than $MF_{0.33}$. This lower amount of Fe and Mg in $MF_{0.33}$-MOSF might affect the adsorption capacity of the impregnated material. EDS result also showed that there were no other element presents in the synthesized material, which confirmed phase purity of the nanomaterials. These results confirmed that the phase pure $MF_{0.33}$ impregnated MOSF nanomaterial had been successfully synthesized in present study.

VSM

Magnetic properties of synthesized $MF_{0.33}$ and $MF_{0.33}$-MOSF nanomaterials were analyzed by vibrating sample magnetometer (VSM) at room temperature with an application of magnetism of − 20,000 to 20,000 Oersted (Oe) (Table S2). The magnetic saturation (Ms), retentivity (Mr) and coercivity (Hc) were found 16.90 emu/g, 1.30 emu/g, 30.15 Oe for pure $MF_{0.33}$ and 1.36 emu/g, 0.14 emu/g, 153.14 Oe for $MF_{0.33}$-MOSF from VSM data respectively. Pure $MgFe_2O_4$ phase showed S-shaped magnetization curve (Fig. 5), which indicated that $MF_{0.33}$ was superparamagnetic material and can be separated easily by an external magnet after adsorption. Conversely, MOSF is a non-magnetic material. After impregnation of $MF_{0.33}$ in MOSF, the new material showed week magnetic properties.

Magnetization saturation of the synthesized nanomaterials was calculated using the formula:

$$\text{Saturation magnetization, Ms} = \varphi mS \qquad (5)$$

where, mS is the saturation moment of a single particle and φ is the volume fraction, it is clear that Ms can be determined by volume fractions and intrinsic properties (saturation moment) of materials involved. Thus, low magnetism of $MF_{0.33}$-MOSF can be attributed to low amount of incorporated $MF_{0.33}$ in it[32]. The magnetic properties decreased after impregnation but magnetic properties of the $MF_{0.33}$-MOSF could be tuned by controlling these two parameters.

Coercivity depends on particle size which will increase up to certain limit with decreasing particle size[33]. Based on BET data, particles size of $MF_{0.33}$ was found 29.95 nm and after impregnation, particle size was 14.05 nm for $MF_{0.33}$-MOSF. Therefore, coercivity increased in $MF_{0.33}$-MOSF than $MF_{0.33}$. The remnant magnetization (Mr) is the magnetization left after removing external magnetic field from a material. The Mr value was found 1.30 emu/g for pure $MF_{0.33}$ and 0.14 emu/g for $MF_{0.33}$ impregnated MOSF. Superparamagnetic $MF_{0.33}$ showed 9.29 times higher Mr than $MF_{0.33}$-MOSF. The ratio of Mr and Ms is called squareness which is important properties for ferromagnetic materials. Depending on processing, Mr/Ms ratio of commercial magnets varied in the range 0.88–0.96[34]. The squareness ratio were found 0.08 and 0.10 for $MF_{0.33}$ and $MF_{0.33}$-MOSF. Because of cubic spinel shape, $MF_{0.33}$ has less Mr/Ms which increased impregnated material.

Zhou et al.[35] found similar magnetization result when synthesized silver phosphate@magnesium ferrite [Ag_3PO_4@$MgFe_2O_4$] nanocomposites. The magnetization of pure $MgFe_2O_4$ material was found 15 emu/g which was decreased to 1.6 emu/g in Ag_3PO_4@$MgFe_2O_4$ (10%). They showed that non-magnetic Ag_3PO_4 attained

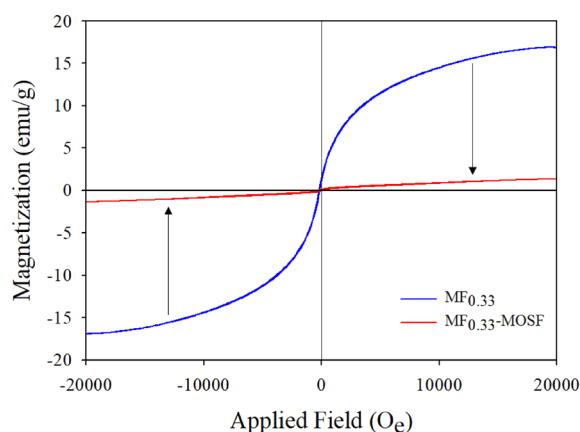**Figure 5.** Magnetization curves of synthesized $MF_{0.33}$ and $MF_{0.33}$-MOSF nanomaterials at room temperature.

good magnetic properties after composite formation with superparamagnetic $MgFe_2O_4$ that can be separated easily from water by a magnet[35]. Khafagy[32] showed that magnetization of pure phase $MgFe_2O_4$ decreased (21.33–5.905 emu/g) when coating $MgFe_2O_4$ with polyaniline. They also found that coercivity decreased 88.66 Oe–81.60 Oe after coating because the particle size of pure $MgFe_2O_4$ (30–35 nm) increased (45 nm) after coating. Hoijang et al.[17] synthesized silica-coated $MgFe_2O_4$ showing superparamagnetic properties. The magnetization of pure $MgFe_2O_4$ and silica-coated $MgFe_2O_4$ were found 37 and 27 emu/g. During synthesis, they added only 1 ml tetraethyl orthosilicate in a solution containing 200 mg of $MgFe_2O_4$. Because of higher amount of $MgFe_2O_4$, the magnetic properties was not decreased much. Therefore, magnetic properties of the nanomaterials synthesized in present study could be increased by changing $MF_{0.33}$ and MOSF ratio.

Comparative study of morphological characteristics

Magnesium ferrite impregnated mesoporous ordered silica foam has been synthesized for the first time under present study. The modified magnesium ferrite nanomaterial showed exceptionally large surface area compared to other modified magnesium ferrite nanomaterials found in literature till date (Table S3). Tiwari and Kaur[36], synthesized silica@magnesium ferrite [SiO_2@$MgFe_2O_4$] material having higher surface area and pore volume than $MF_{0.33}$-MOSF synthesized in this research. But the pore size of SiO_2@$MgFe_2O_4$ material approximately 1.71 times lower than $MF_{0.33}$-MOSF. In addition, complex synthesis process was involved in SiO_2@$MgFe_2O_4$ synthesis. At first they synthesized SiO_2 and $MgFe_2O_4$ nanomaterial. After that further synthesis process was involved for SiO_2@$MgFe_2O_4$ synthesis[36]. Whereas, the synthesis of $MF_{0.33}$-MOSF material was very much simple in present study. At first MOSF synthesized and then this MOSF mixed with other precursor solutions during $MF_{0.33}$ synthesis. Therefore, no further synthesis steps were involved, which could save energy and cost of the research. So, present research successfully synthesized $MF_{0.33}$-MOSF nanomaterial through a simple and cost effective way having large pore size, pore volume and surface area compared to other nanomaterials found in literature (Table S3).

Arsenic adsorption capacity

Adsorption isotherm

Table S4 showed the equilibrium arsenic adsorption isotherm results. The adsorption of both As(III) and As(V) species on synthesized $MF_{0.33}$ and $MF_{0.33}$-MOSF nanomaterial were tried to fit in Langmuir and Freundlich isotherm model (Fig. 6). The fitting results showed that adsorption data was best fitted on Freundlich model based on coefficient of correlation (r^2) data. According to Foo and Hameed[37], Langmuir adsorption isotherm is an
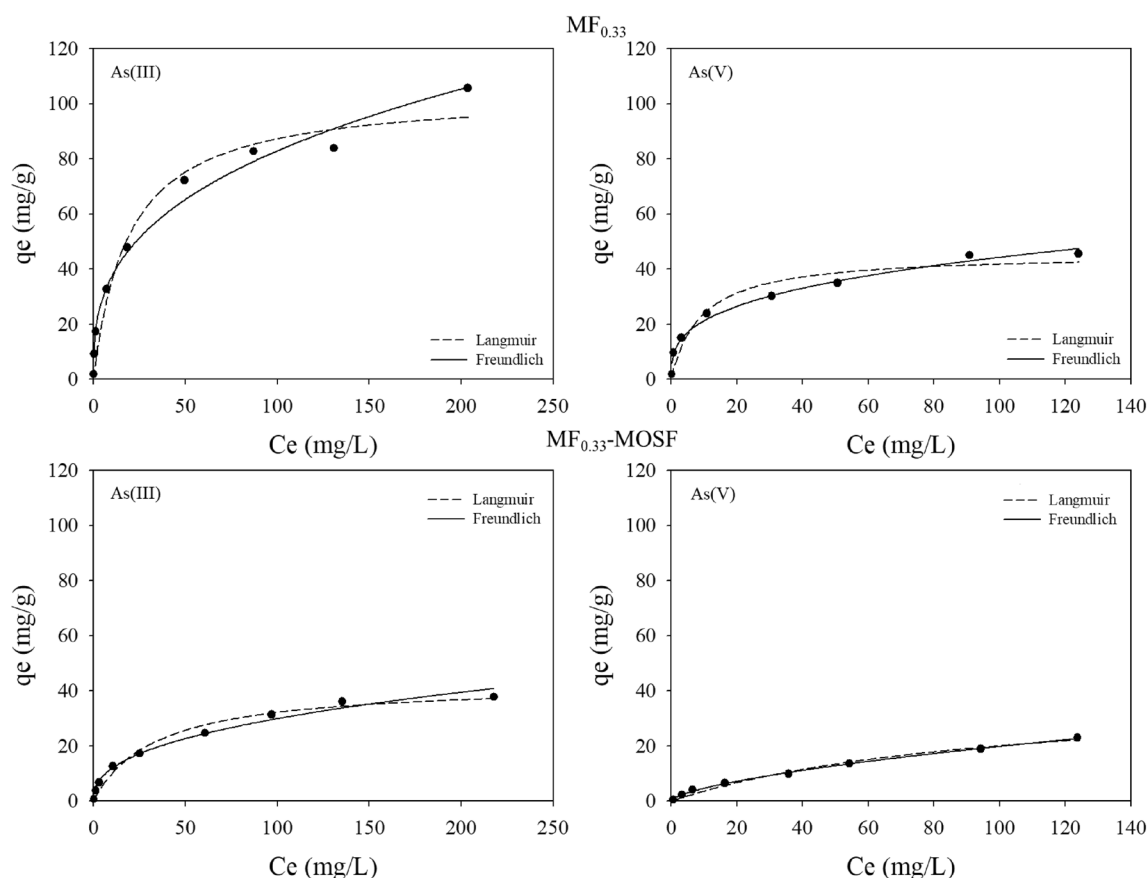

Figure 6. As(III) and As(V) adsorption isotherm of $MF_{0.33}$ and $MF_{0.33}$-MOSF nanomaterial. Conditions: pH = 7, Temperature = 25 °C, adsorbent dose = 1 g/l.

equation based on monolayer adsorption of adsorbate onto adsorbent surface. Besides, Freundlich adsorption isotherm model is based on multilayer adsorption of adsorbate onto heterogeneous surface of the adsorbent which is not restricted to monolayer formation[37,38]. Therefore, multilayer adsorption of both arsenic species was taken place on $MF_{0.33}$ and $MF_{0.33}$-MOSF heterogeneous surface. The heterogeneity factor, $1/n$ can be found from Freundlich model. The value $0.1 < 1/n < 1$ describes efficient adsorption of adsorbate on adsorbent surface[39]. In present study, the parameter $1/n$ calculated from Freundlich model were found 0.34, 0.32 by $MF_{0.33}$ and 0.40, 0.63 by $MF_{0.33}$-MOSF for As(III) and As(V) adsorption, which indicated that both species adsorbed easily on $MF_{0.33}$ and $MF_{0.33}$-MOSF surface[40].

The maximum arsenic adsorption capacity of $MF_{0.33}$ and $MF_{0.33}$-MOSF nanomaterial was found in Langmuir isotherm model. Based on model results, $MF_{0.33}$ and $MF_{0.33}$-MOSF adsorbed 103.94, 42.80 mg/g of As(III) and 45.52, 39.73 mg/g of As(V) at pH 7 respectively. With increasing initial arsenic concentration, adsorption capacity was also increased. At equilibrium, $MF_{0.33}$ nanomaterials adsorbed approximately 2.4 times higher amount of As(III) than $MF_{0.33}$-MOSF. For As(V) adsorption, $MF_{0.33}$ adsorbed slightly higher amount than $MF_{0.33}$-MOSF. As the MOSF showed no arsenic adsorption capacity, $MF_{0.33}$ was totally responsible for arsenic adsorption. Besides that, based on EDS results, $MF_{0.33}$-MOSF contained 2.37 times lower Fe and 2.67 times lower Mg than $MF_{0.33}$ when $MF_{0.33}$-MOSF was synthesized in 1:1 ratio of $MF_{0.33}$ and MOSF. Elemental analysis data by ICP-OES also showed that $MF_{0.33}$-MOSF contain 2.47 times lower Fe and 2.42 times lower Mg than pure $MF_{0.33}$. Therefore, the lower arsenic adsorption capacity was due to lower Fe and Mg content in $MF_{0.33}$-MOSF nanomaterial, which could be enhanced by changing the $MF_{0.33}$ and MOSF ratio.

Adsorption mechanism

Arsenic adsorption on $MF_{0.33}$-MOSF nanomaterial can be discussed based on isotherm data and pH_{PZC} of the material. Adsorption results were well fitted to Freundlich isotherm model indicating that arsenic adsorption occurred on heterogeneous surface of $MF_{0.33}$-MOSF nanomaterial. Therefore, possible mechanism of arsenic adsorption might be through physisorption and chemisorption. In addition, the pH_{PZC} of $MF_{0.33}$-MOSF was found 9.02 which indicated that the nanomaterial surface was positively charged at pH 7 (pH < pH_{PZC}). The available forms of As(III) and As(V) under pH 7 are H_3AsO_3, $H_2AsO_4^-$ and $HAsO_4^{2-}$ which might be easily adsorbed on $MF_{0.33}$-MOSF surface through electrostatic attraction, ion exchange and complex formation. There were two pH_{PZC} (3.31 and 4.78) found for pure MOSF material (Fig. 7). Chrzanowska et al.[41] found pH_{PZC} 4–5.6 of pure mesocellular silica foam. Derylo-Marczewska et al.[42] found pH_{PZC} 4.93 of pure mesoporous silica foam which changed to 6.5 after protein adsorption. Brönsted acidity in silica surface is a well-known properties and pH_{PZC} of these materials was found at a range 2–3 which indicated that silica surface have positive charge (pH < pH_{PZC}) at very lower pH. In addition, after coating with magnetite the pH_{PZC} of modified mesoporous silica changed to 8 which generated positive silica surface[43].

The adsorption experiments under present research were done at pH 7. At this pH, surface of pure MOSF can be regarded negative charged. As result, adsorption capacity of pure MOSF was very much low [(0.58 and 2.49 mg/g for As(III) and As(V) at 1–25 mg/l initial concentrations]. Conversely, pure $MF_{0.33}$ had pH_{PZC} 10.25 which indicated that $MF_{0.33}$ surface showed higher amount of positive sites at pH 7 (pH < pH_{PZC}) which favors arsenic adsorption [(103.94 and 45.52 mg/g for As(III) and As(V)]. After the impregnation of $MF_{0.33}$ in MOSF, pH_{PZC} was changed to 9.02 and adsorption capacity was 42.80 and 39.73 mg/g for As(III) and As(V) respectively. The EDS and elemental analysis data confirmed that $MF_{0.33}$-MOSF contain less Fe and Mg than $MF_{0.33}$, which was the main reason responsible for the lower arsenic adsorption capacity. At pH 7, Arsenous acid (H_3AsO_3) is the available form of As(III) and $H_2AsO_4^-$ and $HAsO_4^{2-}$ are two available forms of As(V) in aqueous solution. So, the $MF_{0.33}$ and $MF_{0.33}$-MOSF nanomaterials having positively charged surface might be easily attached the negatively charged As(V) through complex formation, ion exchange and electrostatic attraction. The possible reactions are:

H_3AsO_3 species of As(III) has no charge which can adsorbed through complex formation. The possible adsorption reactions of As(III) are:
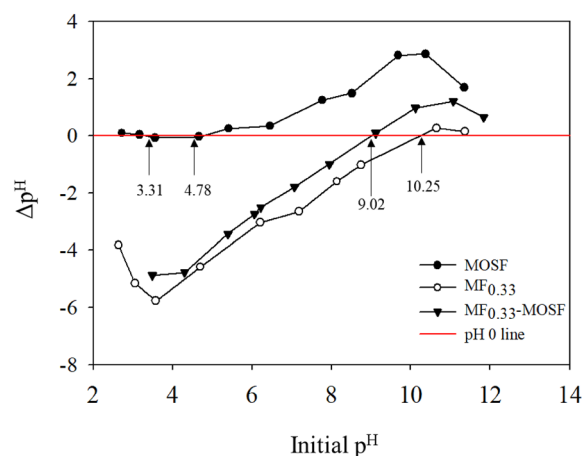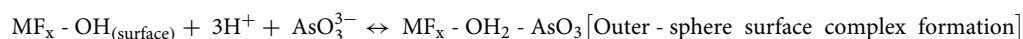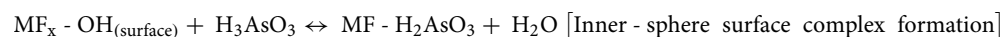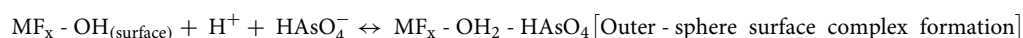

Figure 7. pH_{PZC} of MOSF, $MF_{0.33}$ and $MF_{0.33}$-MOSF nanomaterials.

$$MF_x - OH_{(surface)} + H_3AsO_3 \leftrightarrow MF - H_2AsO_3 + H_2O \left[Inner\text{-}sphere\ surface\ complex\ formation \right]$$

$$MF_x - OH_{(surface)} + 3H^+ + AsO_3^{3-} \leftrightarrow MF_x - OH_2 - AsO_3 \left[Outer\text{-}sphere\ surface\ complex\ formation \right]$$

Possible reactions for $H_2AsO_4^-$ and $HAsO_4^{2-}$ adsorption through chemisorption

$$MF_x - OH_{(surface)} + H^+_{(aq)} \leftrightarrow MF_x\ OH_2^+ \left[at\ pH\ <\ pH_{PZC} \right]$$

$$MF_x - OH_2^+ + H_2AsO_4^- \leftrightarrow MF_x - OH_2 - H_2AsO_4 \left[through\ electrostatic\ attraction \right]$$

$$MF_x - OH_{(surface)} + H_2AsO_4^- \leftrightarrow MF - HAsO_4 + H_2O \left[Inner\text{-}sphere\ surface\ complex\ formation \right]$$

$$MF_x - OH_{(surface)} + H^+ + HAsO_4^- \leftrightarrow MF_x - OH_2 - HAsO_4 \left[Outer\text{-}sphere\ surface\ complex\ formation \right]$$
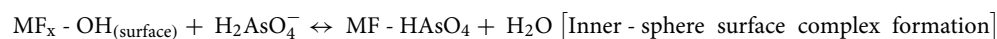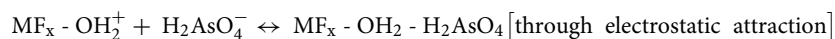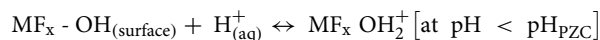
Considering above reactions, chemisorption was the dominant adsorption mechanism for As(III) and As(V) adsorption. Chemisorption process occurred through complex formation, ion exchange and electrostatic attraction. The literature data regarding arsenic oxyanions adsorption on spinal ferrites revealed that the dominant adsorption mechanism was surface complex formation[1,18,38,44–46].

Comparison with other adsorbents for arsenic adsorption
For the first time, magnesium ferrite was impregnated in MOSF which showed enhanced surface area, mesoporous pore size and high pore volume. The material was applied as adsorbent for arsenic removal at pH 7 and 25 °C. The maximum As(III) and As(V) adsorption capacity were found 42.80 and 39.73 mg/g respectively. The material adsorbed higher amount of As(III) and As(V) from water compared to other adsorbents listed in Table S5 at pH 7.

Fe modified activated carbon material showed lower As(III) and As(V) adsorption capacity[4,47]. In addition, longer equilibrium time and membrane filtration with N_2 purging applied for adsorption which limited the research for further application in water treatment. Gupta and Ghosh[48] synthesized Fe(III)-Ti(IV) binary oxide which removed 85 mg/g As(III) within 4.5 h at pH 7. However, the material removed very much lower amount (14 mg/g) of As(V) within 7.5 h at pH 7. In addition, they maintained pH for certain time period until equilibrium reached during adsorption. Furthermore, membrane filtration was applied for separation of adsorbent from water[48]. Fe_3O_4-MnO_2 binary oxide adsorbed 32.13 mg/g As(V) at pH 5[49]. Yu et al.[6] synthesized cellulose@Fe_2O_3 magnetic composites and applied for arsenic removal. The nanocomposites adsorbed 23.16 mg/g As(III) at pH 7.5 and 32.11 mg/g As(V) at pH 2. 3D organized mesoporous silica coated with Fe and Al oxide was synthesized by Glocheux et al.[50] which adsorbed 55 mg/g As(V) at pH 5 and 35 mg/g As(V) at pH 4 respectively. Fe_2O_3/SiO_2 nanocomposite adsorbed only 21.50 mg/g As(III) at pH 7.5 and 14.90 mg/g As(V) at pH 4.5. In both cases, adsorption temperature was 35 °C[51]. Ahangari et al.[52] synthesized nickel-zinc ferrite modified carbon nanotubes nanocomposite for As(V) removal from wastewater. The nickel-zinc ferrite (NZF) and carbon nanotube nickel-zinc ferrite (CNZF) nanocomposites adsorbed 56 and 66 mg/g As(V) at pH 2 and 6 g/l of adsorbent dosage[52]. Therefore, comparing with activated carbon, carbon nanotube, cellulose, binary oxides and other silica modified nanomaterial/nanocomposites, $MF_{0.33}$-MOSF found efficient adsorbent material for As(III) and As(V) removal from water.

Furthermore, magnesium ferrite impregnated MOSF was synthesized following $MF_{0.33}$ synthesis process where MOSF added with precursor materials of $MF_{0.33}$ therefore, no further synthesis process had been applied. For synthesis of other modified materials (Table S3), complex synthesis process were involved which needed higher energy, time and cost. Therefore, based on synthesis, characteristics and adsorption capacity, $MF_{0.33}$-MOSF nanomaterial was considered as one of an ideal material for water treatment. This nanomaterial might work as a green material for sustainable water treatment technology development in future.

Conclusion
Iron based nanomaterials have drawn much attention in adsorptive removal of pollutants from water because of their availability, properties, adsorption capacity, lower cost and ecofriendly nature. Among them, magnesium ferrite nanomaterials showed greater properties and performance in water treatment process. However, being a nanomaterial, it has limitations such as stability, aggregate formation and separation. Therefore, modification of magnesium ferrite nanomaterials with well-structured materials having higher stability, surface area and easy separation from solution are very much popular in recent time. Following that, a new combination, $MF_{0.33}$-MOSF has been successfully synthesized and applied for As(III) and As(V) removal from water at pH 7. MOSF having negatively charged surface area at pH 7 showed repulsion against arsenic oxyanions. However, adsorption properties were increased after impregnation with $MF_{0.33}$. The magnetic $MF_{0.33}$-MOSF showed better morphological properties and adsorption capacity (at pH 7) compared to other nanomaterials found in literature. Adsorption results best fitted with Freundlich isotherm and adsorption mechanism was found to chemical sorption through complex formation and electrostatic attraction on heterogeneous surface. Modification of $MF_{0.33}$ with MOSF using simple, less time-consuming and cost-effective procedure was successfully confirmed to be effective. Therefore, magnetic $MF_{0.33}$-MOSF composites could be competitive nanoadsorbents for arsenic removal from water.

Data availability
Research data and materials are available upon request from the corresponding author and following journal guideline.

References

1. Uddin, M. J. & Jeong, Y. K. Review: Efficiently performing periodic elements with modern adsorption technologies for arsenic removal. *Environ. Sci. Pollut. Res.* **27**, 39888–39912 (2020).
2. Uddin, M. J. & Jeong, Y. K. Adsorptive removal of pollutants from water using magnesium ferrite nanoadsorbent: A promising future material for water purification. *Environ. Sci. Pollut. Res.* **29**, 9422–9447 (2022).
3. Hao, L., Liu, M., Wang, N. & Li, G. A critical review on arsenic removal from water using iron-based adsorbents. *RSC Adv.* **8**, 39545–39560 (2018).
4. Zhu, H., Jia, Y., Wu, X. & Wang, H. Removal of arsenic from water by supported nano zero-valent iron on activated carbon. *J. Hazard. Mater.* **172**, 1591–1596 (2009).
5. Li, Y., Jin, Z., Li, T. & Xiu, Z. One-step synthesis and characterization of core–shell Fe@SiO2 nanocomposite for Cr (VI) reduction. *Sci. Total Environ.* **421–422**, 260–266 (2012).
6. Yu, X. *et al.* One-step synthesis of magnetic composites of cellulose@iron oxide nanoparticles for arsenic removal. *J. Mater. Chem. A* **1**, 959–965 (2013).
7. Uddin, M. J., Ampiaw, R. E. & Lee, W. Adsorptive removal of dyes from wastewater using a metal-organic framework: A review. *Chemosphere* **284**, 131314 (2021).
8. Baig, S. A., Sheng, T., Hu, Y., Xu, J. & Xu, X. Arsenic removal from natural water using low cost granulated adsorbents: A review. *Clean Soil Air Water* **43**, 13–26 (2015).
9. Asere, T. G., Stevens, C. V. & Du Laing, G. Use of (modified) natural adsorbents for arsenic remediation: A review. *Sci. Total Environ.* **676**, 706–720 (2019).
10. Yang, J. W. *et al.* Functionalized mesoporous silicon nanomaterials in inorganic soil pollution research: Opportunities for soil protection and advanced chemical imaging. *Curr. Pollut. Rep.* **6**, 264–280 (2020).
11. Al-Shehri, B. M., Khder, A. E. R. S., Ashour, S. S. & Hamdy, M. S. A review: The utilization of mesoporous materials in wastewater treatment. *Mater. Res. Express* **6**, 12 (2019).
12. Yang, J. *et al.* Rationally designed functional macroporous materials as new adsorbents for efficient phosphorus removal. *J. Mater. Chem.* **22**, 9983–9990 (2012).
13. Yang, J. *et al.* High-content, well-dispersed γ-Fe2O3 nanoparticles encapsulated in macroporous silica with superior arsenic removal performance. *Adv. Funct. Mater.* **24**, 1354–1363 (2014).
14. Uddin, M. J. & Jeong, Y. Application of magnesium ferrite nanomaterials for adsorptive removal of arsenic from water : Effects of Mg and Fe ratio. *Chemosphere* **307**, 135817 (2022).
15. Jung, K. W., Lee, S. & Lee, Y. J. Synthesis of novel magnesium ferrite (MgFe2O4)/biochar magnetic composites and its adsorption behavior for phosphate in aqueous solutions. *Bioresour. Technol.* **245**, 751–759 (2017).
16. Karthikeyan, P., Elanchezhiyan, S. S., Meenakshi, S. & Park, C. M. Magnesium ferrite-reinforced polypyrrole hybrids as an effective adsorbent for the removal of toxic ions from aqueous solutions: Preparation, characterization, and adsorption experiments. *J. Hazard. Mater.* **408**, 124892 (2021).
17. Hoijang, S. *et al.* Silica-coated magnesium ferrite nanoadsorbent for selective removal of methylene blue. *Colloids Surf. A Physicochem. Eng. Asp.* **606**, 125483 (2020).
18. Wu, C. *et al.* Defective magnesium ferrite nano-platelets for the adsorption of As(V): The role of surface hydroxyl groups. *Environ. Pollut.* **235**, 11–19 (2018).
19. Tang, W., Su, Y., Li, Q., Gao, S. & Shang, J. K. Superparamagnetic magnesium ferrite nanoadsorbent for effective arsenic (III, V) removal and easy magnetic separation. *Water Res.* **47**, 3624–3634 (2013).
20. Nonkumwong, J. *et al.* Phase formation, morphology and magnetic properties of MgFe2O4 nanoparticles synthesized by hydrothermal technique. *J. Magn. Magn. Mater.* **381**, 226–234 (2015).
21. Wang, H. *et al.* Supra-assembly of siliceous vesicles. *J. Am. Chem. Soc.* **128**, 15992–15993 (2006).
22. Nasir, A. M., Md-Nordin, N. A. H., Goh, P. S. & Ismail, A. F. Application of two-dimensional leaf-shaped zeolitic imidazolate framework (2D ZIF-L) as arsenite adsorbent: Kinetic, isotherm and mechanism. *J. Mol. Liq.* **250**, 269–277 (2018).
23. Kaur, M., Kaur, N., Jeet, K. & Kaur, P. MgFe2O4 nanoparticles loaded on activated charcoal for effective removal of Cr(VI)– A novel approach. *Ceram. Int.* **41**, 13739–13750 (2015).
24. Tatarchuk, T. *et al.* Magnesium-zinc ferrites as magnetic adsorbents for Cr(VI) and Ni(II) ions removal: Cation distribution and antistructure modeling. *Chemosphere* **270**, 129414 (2021).
25. Zhao, C., Yang, J., Wang, Y. & Jiang, B. Well-dispersed nanoscale zero-valent iron supported in macroporous silica foams: Synthesis, characterization, and performance in Cr(VI) removal. *J. Mater.* **2017**, 1–13 (2017).
26. Dui, J., Zhu, G. & Zhou, S. Facile and economical synthesis of large hollow ferrites and their applications in adsorption for as(V) and Cr(VI). *ACS Appl. Mater. Interfaces* **5**, 10081–10089 (2013).
27. Shen, Y., Wu, Y., Li, X., Zhao, Q. & Hou, Y. One-pot synthesis of MgFe2O4 nanospheres by solvothermal method. *Mater. Lett.* **96**, 85–88 (2013).
28. Zhao, L. *et al.* Synthesis, characterization and adsorptive performance of MgFe2O4 nanospheres for SO2 removal. *J. Hazard Mater.* **184**, 704–709 (2010).
29. Ilhan, S., Izotova, S. G. & Komlev, A. A. Synthesis and characterization of MgFe2O4 nanoparticles prepared by hydrothermal decomposition of co-precipitated magnesium and iron hydroxides. *Ceram. Int.* **41**, 577–585 (2015).
30. Huang, K. & Cai, Z. Synthesis and characterization of three-dimensional ordered macroporous Si–Al compound oxide by sol–gel process. *J. Sol-Gel Sci. Technol.* **87**, 264–268 (2018).
31. Wang, H. *et al.* Controlled synthesis of hexagonal mesostructure silica and macroporous ordered siliceous foams for VOCs adsorption. *RSC Adv.* **5**, 5695–5703 (2015).
32. Khafagy, R. M. Synthesis, characterization, magnetic and electrical properties of the novel conductive and magnetic Polyaniline/MgFe2O4 nanocomposite having the core-shell structure. *J. Alloys Compd.* **509**, 9849–9857 (2011).
33. Kotnala, R. K. & Shah, J. Ferrite Materials: Nano toSpintronics Regime. *Handbook of Magnetic Materials* (Elsevier, 2015).
34. De Campos, M. F., Da Silva, F. A. S., Perigo, E. A. & De Castro, J. A. Stoner-wohlfarth model for the anisotropic case. *J. Magn. Magn. Mater.* **345**, 147–152 (2013).
35. Zhou, T. *et al.* Efficient degradation of rhodamine B with magnetically separable Ag3PO4@MgFe2O4 composites under visible irradiation. *J. Alloys Compd.* **735**, 1277–1290 (2018).
36. Tiwari, S. & Kaur, M. Mechanistic insight into structural and adsorptive properties of core shell reversal nanocomposites of rice husk silica and magnesium ferrite. *Adv. Powder Technol.* **31**, 2315–2326 (2020).

37. Foo, K. Y. & Hameed, B. H. Insights into the modeling of adsorption isotherm systems. *Chem. Eng. J.* **156**, 2–10 (2010).
38. Hu, Q., Liu, Y., Gu, X. & Zhao, Y. Adsorption behavior and mechanism of different arsenic species on mesoporous MnFe2O4 magnetic nanoparticles. *Chemosphere* **181**, 328–336 (2017).
39. Alghamdi, A. A. *et al.* Efficient adsorption of lead (II) from aqueous phase solutions using polypyrrole-based activated carbon. *Mater. Basel.* **12**, 12 (2019).
40. Sun, T. *et al.* Efficient removal of arsenite through photocatalytic oxidation and adsorption by ZrO2-Fe3O4 magnetic nanoparticles. *Appl. Surf. Sci.* **416**, 656–665 (2017).
41. Chrzanowska, A., Derylo-Marczewska, A. & Wasilewska, M. Mesocellular silica foams (Mcfs) with tunable pore size as a support for lysozyme immobilization: Adsorption equilibrium and kinetics, biocomposite properties. *Int. J. Mol. Sci.* **21**, 1–22 (2020).
42. Deryło-Marczewska, A., Chrzanowska, A. & Marczewski, A. W. Morphological, structural and physicochemical characteristics of the surface of mesocellular silica foam with the adsorbed OVA and BSA proteins. *Micropor. Mesopor. Mater.* **293**, 109769 (2020).
43. Dorigon, L. *et al.* Synthesis and characterization of mesoporous silica-coated magnetite containing cetyltrimethylammonium bromide and evaluation on the adsorption of sodium dodecylbenzenesulfonate. *Appl. Surf. Sci.* **420**, 954–962 (2017).
44. Zhou, J. *et al.* Adsorption behavior and mechanism of arsenic on mesoporous silica modified by iron-manganese binary oxide (FeMnOx/SBA-15) from aqueous systems. *J. Hazard. Mater.* **384**, 121229 (2020).
45. Reddy, D. H. K. & Yun, Y. S. Spinel ferrite magnetic adsorbents: Alternative future materials for water purification?. *Coord. Chem. Rev.* **315**, 90–111 (2016).
46. Xu, W. H. *et al.* Superparamagnetic mesoporous ferrite nanocrystal clusters for efficient removal of arsenite from water. *Cryst. Eng. Commun.* **15**, 7895–7903 (2013).
47. Payne, K. B. & Abdel-Fattah, T. M. Adsorption of arsenate and arsenite by iron-treated activated carbon and zeolites: Effects of pH, temperature, and ionic strength. *J. Environ. Sci. Heal. Part A Toxic/Hazardous Subst. Environ. Eng.* **40**, 723–749 (2005).
48. Gupta, K. & Ghosh, U. C. Arsenic removal using hydrous nanostructure iron(III)-titanium(IV) binary mixed oxide from aqueous solution. *J. Hazard Mater.* **161**, 884–892 (2009).
49. Zhao, Z., Liu, J., Cui, F., Feng, H. & Zhang, L. One pot synthesis of tunable Fe3O4-MnO2 core-shell nanoplates and their applications for water purification. *J. Mater. Chem.* **22**, 9052–9057 (2012).
50. Glocheux, Y. *et al.* Adsorption study using optimised 3D organised mesoporous silica coated with Fe and Al oxides for specific As(III) and As(V) removal from contaminated synthetic groundwater. *Micropor. Mesopor. Mater.* **198**, 101–114 (2014).
51. Zeng, L. Arsenic adsorption from aqueous solutions on an Fe(III)-Si binary oxide adsorbent. *Water Qual. Res. J. Can.* **39**, 267–275 (2004).
52. Ahangari, A., Raygan, S. & Ataie, A. Capabilities of nickel zinc ferrite and its nanocomposite with CNT for adsorption of arsenic (V) ions from wastewater. *J. Environ. Chem. Eng.* **7**, 103493 (2019).

Author contributions

All authors contributed to the study conception and design. Nanomaterials preparation, adsorption experiments and analysis were performed by M.J.U. English check and further corrections were made by Professor Y.-K.J. All authors read and approved the final manuscript. Upon acceptance all authors are agreed to publish the article in *Scientific Reports*.

Funding

Competing interests

The authors declare no competing interests.

Additional information

Supplementary Information The online version contains supplementary material available at https://doi.org/10.1038/s41598-023-48327-7.

Correspondence and requests for materials should be addressed to M.J.U. or Y.-K.J.

Reprints and permissions information is available at www.nature.com/reprints.

Publisher's note Springer Nature remains neutral with regard to jurisdictional claims in published maps and institutional affiliations.